IEEE Access
Multidisciplinary | Rapid Review | Open Access Journal

Received 16 August 2023, accepted 29 August 2023, date of publication 7 September 2023, date of current version 13 September 2023.

Digital Object Identifier 10.1109/ACCESS.2023.3312171

RESEARCH ARTICLE

Design of a Modular Pipeline Robot Structure and Passing Ability Analysis

QING LI AND WENYA ZHAO
School of Mechanical Engineering, Tianjin University, Tianjin 300350, China
Corresponding author: Wenya Zhao (wenya_zhao@tju.edu.cn)

ABSTRACT To date, scholars have only conducted theoretical research on pipeline robots with cylindrical shapes over bends. However, not all pipeline robots are cylindrical in shape. This paper presents a theoretical investigation of a rectangular pipeline robot's bending-passing ability using geometric and vector approaches and addresses dimensional limitations. Considering the shortcomings of most existing pipeline robots, such as the limited range of pipe diameters that are allowed, the inability to climb vertical pipes, and the single purpose, this study suggests a multi-functional modular pipeline robot that can support a wide range of pipe diameters. The drive module was constructed as a rectangular structure, which confirmed the accuracy of the bend-through theory. The driving module, as the central component of the pipeline robot, can accommodate pipe diameters ranging from 250 to 450mm. It was demonstrated that it can generate a traction force of approximately 600N, which can be used to drive other working modules.

INDEX TERMS Climbing robots, motion analysis, snake robots, systems simulation.

I. INTRODUCTION

Owing to their high level of safety when transporting substances such as oil and gas, pipeline transportation has become a popular mode of transportation. Pipelines that develop cracks may become defective with age [1]. These weaknesses pose a substantial risk of media leakage, endangering both public safety and ecological security [2], [3]. In most situations, manual labor is not an option because of the constraints imposed by the pipeline environment and size. Consequently, it is vital to regularly monitor pipelines using appropriate instruments. At present, the use of pipeline robots to inspect and work on pipelines is convenient, safe, and labor-saving.

According to their motion mechanisms, pipeline robots are classified as wheeled [4], crawler [5], spiral [6], serpentine [7], geometrid [8], and passive [9]. Pipeline environments in which pipeline robots operate are complex. The ability of a robot to pass through a pipeline is a key sign of its performance. Common types of pipes include bends, vertical pipes, and straight horizontal pipes. The robot must be built to comply with the geometric requirements of the pipe if it passes through pipes such as bends. The robot's bending-passing ability is the ability of the robot to pass the bend smoothly within the constraints of the pipe geometry. Most pipeline robots are cylindrical in shape. Scholars have only conducted theoretical research or adopted theoretical conclusions for cylindrical pipeline robots traveling through a bend to determine whether the pipeline robot can pass through the bend [10], [11], [12]. The robot in the pipeline is not cylindrical, and some of it changes its shape to become rectangular [13]. The theory of the passing ability of cylindrical robots is used to verify whether rectangular pipe robots can pass bent pipes successfully. The parameters of the rectangular pipe robot cannot be accurately determined in this way. Therefore, theoretical analysis of the size limitation of a rectangular pipe robot through a bend is required.

The motion mechanism of the robot in the pipeline was designed to enhance its versatility [14]. Pipeline robots with a shape similar to that of a car [15], which can crawl in horizontal pipes, cannot climb vertical pipes and cannot ensure the alignment of the robot body with the pipes. Therefore, press-wall pipeline robots [16] have received considerable attention. The wall-pressing mechanism of wall-pressing pipeline robots is the basis of their ability to adapt to different pipe diameters. The crawler pipe robot developed

The associate editor coordinating the review of this manuscript and approving it for publication was Wai-keung Fung.

TABLE 1. Adaptability of pipeline robots.

Ref.	Applicable pipe diameter (mm)	Reducer coefficient	The shape of the pipe
[4]	480-600	0.25	--
[6]	209	0	X/Y/L
[17]	600-800	0.33	--
[21]	150-200	0.333	X/Y/L
[20]	101.6-152.4	0.5	X/Y/L
[18]	1200-1500	0.25	X
[19]	180-210	0.166	X/L/37°
[22]	60-90	0.5	X/Y/L
[23]	550-714	0.298	X
[24]	200	0	X
[25]	270-350	0.296	--

X-horizontal pipe, Y-vertical pipe, L-90° bend, T-T-shaped pipe, °-climbing slope.

by the Kyungbuk Institute of Science and Technology in Daegu, Korea [17] has an adaptive active reducer mechanism that can inspect and clean pipes between 600-800 mm. Feng et al. [18] designed a wheeled wall press mechanism with variable diameters using a screw-nut sub, enabling the robot to accommodate pipe diameters in the range 1200-1500 mm. Yan et al. [19] designed a pipe robot with two support mechanisms, capable of accommodating pipe diameters in the range 180-210 mm. The body size of the robot increases because of the adoption of the wall compression mechanism, which is unfavorable for the pipe robot to pass through the bends. Kakogawa and Ma [20] designed an in-pipe inspection module called AIR0-2.3s. The module has an omnidirectional bend adaptive mechanism that can smoothly pass through bends. The MRINSPECT wheeled pipeline robot from Sungkyunkwan University can make the robot smaller with its special reducer mechanism to achieve a 150-200 mm reducer [21]. Table 1 shows the pipeline adaptation of pipeline robots in recent years, the pipe diameter adaptation of pipeline robots by the reducer range and reducer coefficient, and the pipe passage of pipeline robots by their adapted pipe shapes. Most of the current pipeline robot reducer coefficients are below 0.5. Moreover, their ability to climb vertical pipes was weak. In this study, a cylinder reducer was designed such that the reducer mechanism is in the main body of the robot, which makes the robot mechanism more compact and can have the characteristics of a strong driving force.

Most pipeline robots can only be employed under specified conditions. Most of these have only a single function [26]. Some robots offer defect detection functions, such as crack identification in aged pipes [25], [27], [28], [29], [30]. A pipe grinding robot may polish the welding beads and seams that develop during the pipe welding process to remove impediments and clean the pipe [23], [31]. Some contaminants accumulated inside long-used pipes, such as dust and oil, can be cleaned using in-pipe cleaning robot [18], [32]. If the contaminants are not cleaned in time, they will have an impact on the pipeline transportation environment and efficiency.

According to the research, there is a deficiency in the theory of pipeline robot bending passing ability. There is

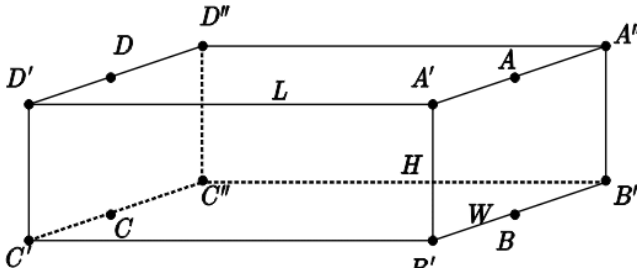

FIGURE 1. The model of the rectangular body.

no theoretical research on the passing ability of rectangular pipeline robots. Concerning the form and function of pipeline robots, they adapt to a small range of pipes (small reducer coefficient of pipeline robots) and most of them have only one function. In response to these issues, the following work was conducted in this study:

(1) This paper presents a theoretical study of the bending-passing ability of rectangular robots using the vector method in Section II.

(2) In Section III, a multi-functional serpentine pipeline robot that can support a wide range of pipe diameters is built based on the modular design concept. The drive module, as the core of the robot, examines the accuracy of the rectangular pipe robot going through a bent pipe. Furthermore, the drive module can adapt to a diameter ranging from 250 to 450mm (reducer coefficient of 0.8) and be linked to the different modules via bi-directional universal joints to create a robot with different operating functions.

(3) The robot model is theoretically studied and simulated for validation in Sections IV and V. The pipeline robot is validated experimentally in Section VI. The magnitude of the traction force generated by the robot is measured.

II. THE PASSING ABILITY OF RECTANGULAR ROBOTS AT THE BEND

The size restrictions for rectangular robots differ from those for traditional cylindrical robots up to a specific radius of curvature. The maximum length of the robot must be considered when designing a structure. In this section, the geometric method is used to model the pipeline robot through the bent pipe, and the vector method is used to theoretically derive the capacity limit of the rectangular robot through the bent pipe.

A. MATHEMATICAL MODEL

This section uses a geometric method to abstract the rectangular pipeline robot as a standard rectangle. Figure 1 shows a schematic of a pipe robot with a rectangular body. W is the robot width, H height, and L length. A', B', C', D', A'', B'', C'', and D'' are the eight vertices of the cuboid. A, B, C, and D are midpoints of $A'A''$, $B'B''$, $C'C''$, and $D'D''$.

Take plane $ABCD$ as plane a. The plane over the axis of the pipe is taken as the plane b. Because a pipe robot generally adopts a symmetrical structure, the plane a and plane b coincide during the robot over the bend, as shown in Figure 2.

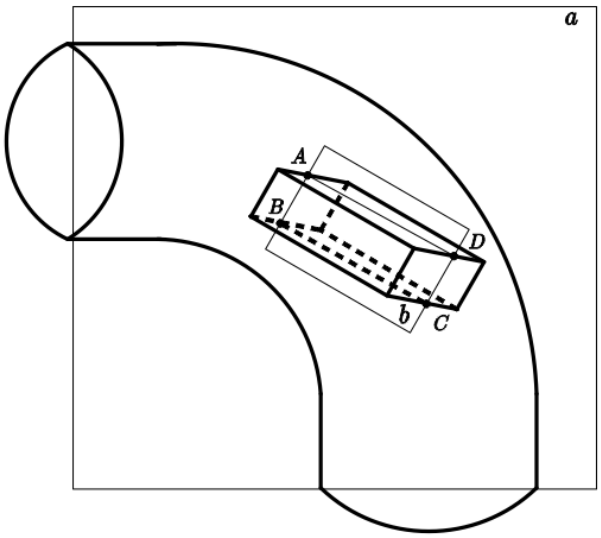

FIGURE 2. Model of the robot when crossing the bend.

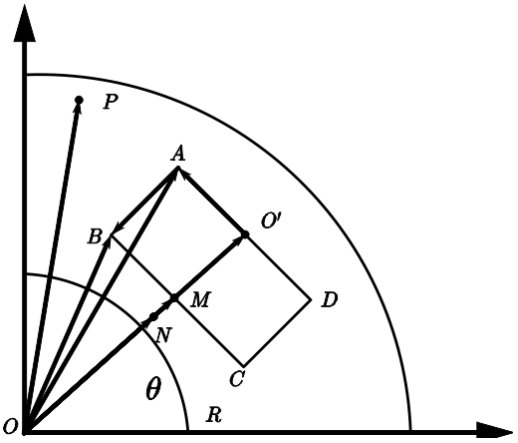

FIGURE 3. Interference along the centerline.

B. THEORETICAL ANALYSIS

The ability of the robot to effectively navigate a bend is determined by whether its body interacts with the pipe's inner wall when it passes through the bend. As a result, when the robot passes through the bend pipe, its size is limited by the geometry of the bent pipe. The size of the robot that can fit through the bend is determined in this section by considering the constraint that it cannot interfere with the inner wall of the pipe.

1) WHEN THE ROBOT FOLLOWS THE CENTERLINE OF THE PIPE

In the plane a, the robot is in the shape of a rectangle. The interference is shown in Figure 3. θ is the angle between $\mathbf{OO}'$ and the x-axis.

$$AB = CD = H \tag{1}$$

$$AD = BC = L \tag{2}$$

Because the robot's end face is rectangular, points A, B, C, D, and M cannot come into contact with the inner wall. When the end face is positioned to contact the pipe wall, point N is the limited position of the point M. When the upper-end face of the robot meets the pipe wall, point P is the limit position of point A and D. Figure 4 shows the relationship between point N, P,and the pipe wall.

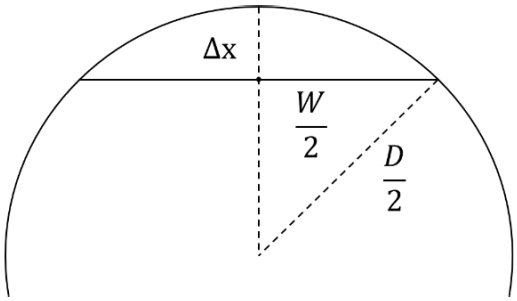

FIGURE 4. Limitation of interference at the endpoint.

The inner and outer walls of the pipe were separated from the points N and P by the following distances:

$$\Delta x = \frac{D}{2} - \sqrt{\left(\frac{D}{2}\right)^2 - \left(\frac{W}{2}\right)^2} \tag{3}$$

To determine the limit dimensions of the rectangular pipe robot over the bend, it is necessary to consider the limit situations of each endpoint and end face where the robot may interfere with the inner wall of the pipe. This study focuses on whether the five points A', B', C', D' and M interfere with the inner wall of the pipe. The interference example of a cylindrical pipe robot over a bend was derived from the literature [33] using the vector approach. Some of the findings can be applied to the rectangular pipe robot in this study. According to the literature [33], the apex of the end face where M is located cannot be close to the inner wall when A' and D' make contact with the outer wall. B' and C' cannot contact the inner wall when the apex of the end face where M is located touches it. A' and D' cannot contact the tube wall simultaneously, as does B' and C'. Consequently, as long as A' and D' do not interfere, the robot does not come into contact with the wall. In other words, the distance between A, D and the outside wall is greater than that of Δx.

The following vectors can be obtained from Figure 3:

$$\mathbf{OO}' = \left[\left(R + \frac{H}{2}\right)\cos\theta, \left(R + \frac{H}{2}\right)\sin\theta\right] \tag{4}$$

$$\mathbf{O}'\mathbf{A} = \left[-\frac{L}{2}\sin\theta, \frac{L}{2}\cos\theta\right] \tag{5}$$

$$\begin{aligned}\mathbf{OA} &= \mathbf{OO}' + \mathbf{O}'\mathbf{A} \\ &= \left[\left(R+\frac{H}{2}\right)\cos\theta - \frac{L}{2}\sin\theta, \left(R+\frac{H}{2}\right)\sin\theta + \frac{L}{2}\cos\theta\right]\end{aligned} \tag{6}$$

$$|\mathbf{OA}| = \sqrt{\left(R + \frac{H}{2}\right)^2 + \left(\frac{L}{2}\right)^2} \tag{7}$$

$$|\mathbf{OP}| = R + \frac{D}{2} - \Delta x \tag{8}$$

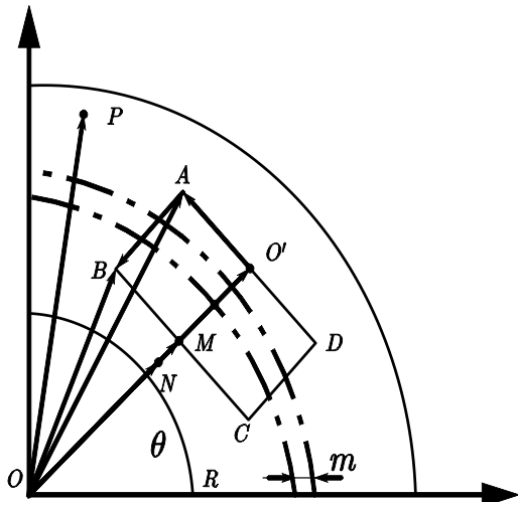

FIGURE 5. Interference at eccentricity.

A, *D* does not touch the outer wall or touches the outer wall under the following conditions:

$$R+\frac{D}{2}-\Delta x\geq\sqrt{\left(R+\frac{H}{2}\right)^2+\left(\frac{L}{2}\right)^2} \tag{9}$$

Reduced to:

$$L\leq 2\sqrt{\left(R+\frac{D}{2}-\Delta x\right)^2-\left(R+\frac{H}{2}\right)^2} \tag{10}$$

2) WHEN THE ROBOT FOLLOWS THE ECCENTRIC LINE OF THE PIPE

The eccentricity has been set to m. The interference is shown in Figure 5.

When the eccentricity is negative ($m \geq 0$), the pipe robot leans toward the inner wall.

The following vectors can be obtained:

$$\left|\mathbf{OO'}\right|=R-m+\frac{H}{2} \tag{11}$$

$$\mathbf{OO'}=\left[\left(R-m+\frac{H}{2}\right)\cos\theta,\left(R-m+\frac{H}{2}\right)\sin\theta\right] \tag{12}$$

$$\mathbf{O'A}=\left[-\frac{L}{2}\sin\theta,\frac{L}{2}\cos\theta\right] \tag{13}$$

$$\begin{aligned}\mathbf{OA}&=\mathbf{OO'}+\mathbf{O'A}\\&=\left[\left(R-m+\frac{H}{2}\right)\cos\theta-\frac{L}{2}\sin\theta,\right.\\&\quad\left.\left(R-m+\frac{H}{2}\right)\sin\theta+\frac{L}{2}\cos\theta\right]\end{aligned} \tag{14}$$

$$\left|\mathbf{OA}\right|=\sqrt{\left(R-m+\frac{H}{2}\right)^2+\left(\frac{L}{2}\right)^2} \tag{15}$$

When the top point of the end face where M is located is in contact with the inner wall of the pipe:

$$\left|\mathbf{OM}\right|=\left|\mathbf{ON}\right| \tag{16}$$

$$\left|\mathbf{OM}\right|=R-m-\frac{H}{2} \tag{17}$$

$$\left|\mathbf{ON}\right|=R-\frac{D}{2}+\Delta x \tag{18}$$

Based on the above equation, the following conclusions can be gotten:

$$m=\frac{D-H}{2}-\Delta x \tag{19}$$

Because of $|OP| \geq |OA|$, the following conclusions can be gotten:

$$R+\frac{D}{2}-\Delta x\geq\sqrt{\left(R-m+\frac{H}{2}\right)^2+\left(\frac{L}{2}\right)^2} \tag{20}$$

Reduced to:

$$L\leq 2\sqrt{\left(R+\frac{D}{2}-\Delta x\right)^2-\left(R-\frac{D}{2}+H+\Delta x\right)^2} \tag{21}$$

When the top point of the end face where M is located is in contact with the inner wall of the pipe, $|OM| \geq |ON|$. The following conclusions were drawn:

$$m<\frac{D-H}{2}-\Delta x \tag{22}$$

$$R+\frac{D}{2}-\Delta x\geq\sqrt{\left(R-m+\frac{H}{2}\right)^2+\left(\frac{L}{2}\right)^2} \tag{23}$$

The vertex of the end face where M is placed does not contact the inner wall. Whether A' and D' make contact with the outer wall depends m value.

When the eccentricity is positive ($m \geq 0$), the pipe robot leans toward the outer wall. The following vectors can be obtained:

$$\left|\mathbf{OM}\right|=R+m-\frac{H}{2} \tag{24}$$

$$\left|\mathbf{ON}\right|=R-\frac{D}{2}+\Delta x \tag{25}$$

Because of $|OM| \geq |ON|$, the following conclusions can be gotten:

$$m\geq\frac{H-D}{2}+\Delta x \tag{26}$$

This equation is a constant. $|OP| \geq |OA|$ determines whether A' and D' touch the outer wall, and is expressed as follows:

$$R+\frac{D}{2}-\Delta x\geq\sqrt{\left(R-m+\frac{H}{2}\right)^2+\left(\frac{L}{2}\right)^2} \tag{27}$$

C. CONCLUSION ANALYSIS

According to [34], the equation for a cylindrical pipeline robot is as follows:

$$L_{\max}=2\sqrt{\left(R+\frac{D}{2}\right)^2-\left(R-\frac{D}{2}+d\right)^2} \tag{28}$$

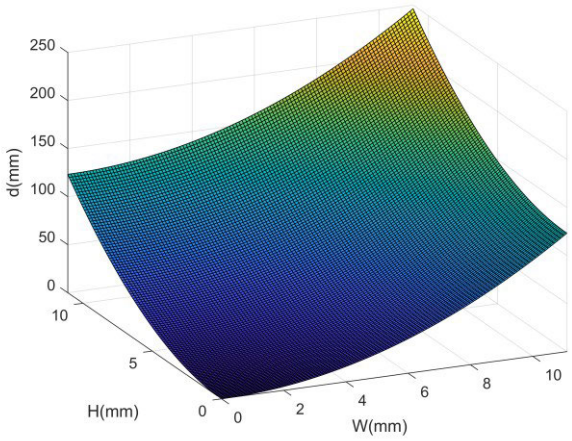

FIGURE 6. The relationship between d and W and H.

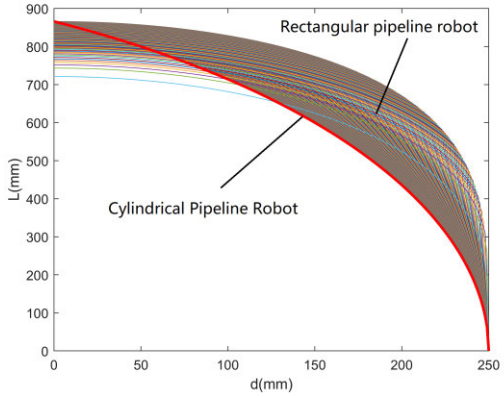

FIGURE 7. Formula Comparison.

The relationship between the dimensions W, H, and d of the rectangular pipeline robots, which can adapt to a 250 mm pipe, is shown in Figure 6. Multiple cases may have the same d value. The ultimate length of the rectangular pipeline robot is related to the values of W and H. The dimensional profiles of cylindrical and rectangular duct robots are compared in Figure 7. The limit length of a rectangular pipeline robot is related to the values of W and H. The limit dimension curves of pipeline robots. As shown in Figure 7, the limit length of the rectangular pipeline robot differed significantly from that of the cylindrical pipeline robot when the same value of d was considered. Therefore, the size limit of the pipeline robot can be determined more accurately using the size restriction equation [34] provided in this study. The available space can be better utilized, which is advantageous for pipe robot design.

III. DESIGN OF MECHANICAL STRUCTURES

A modular pipeline robot consists of several modules. Each robot component has an independent function and can be rented from the other in one or more ways to achieve a whole with new functions [35]. Modularity can reduce production and maintenance costs. Based on the concept of modularity, a multi-functional serpentine pipeline robot that can support a wide range of pipe diameters was created in this study. The

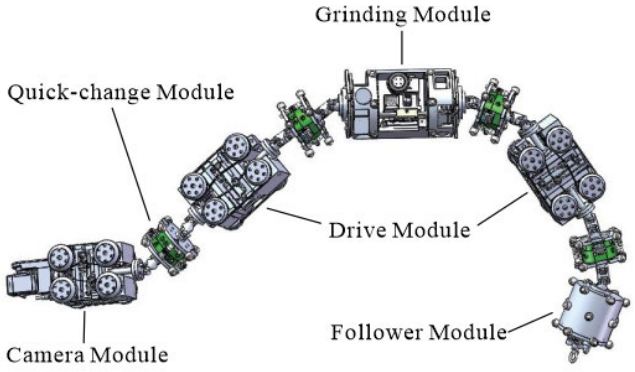

FIGURE 8. The overall structure of the robot.

modules of this robot perform various functions. Modules can be constructed based on these requirements. This section presents a structural design for the drive module based on the dimensional restrictions for rectangular pipe robots across bends.

A. OVERALL STRUCTURE OF THE ROBOT

The overall structure of the pipeline robot is shown in Figure 8. The drive module, camera module, scanning module, clamping module, grinding module, dust vacuuming, and rolling module are the six main modules that make up the medium-sized pipeline detection and cleaning robot. The drive module ensures that the robot has a sufficient torque to move. The most user-friendly inspection module for a robot is the camera module, which examines the pipe and provides basic conclusions regarding its interior. The scanning module delivers circumferential measurements of the pipe and identifies the internal pipe problems. To ensure smooth passage of the robot, a picking module was employed to remove large foreign objects from inside the pipe. The pipe wall can be polished inside the pipe owing to the ability of the grinding module to handle the pipe flaws. To ensure the cleanliness of the pipeline's inner wall and support the long-term steady and safe operation of the nuclear pipeline, dust-absorbing and sweeping modules remove small foreign items from inside the pipeline. Each module is quick to replace and capable of carrying out a specified task. For various pipeline operation requirements, the related modules can be changed quickly and effectively.

B. DRIVE MODULE DESIGN

The drive module is the most crucial component of the robot because it can ensure that the robot has sufficient force to move and is essential for climbing vertical pipes. The reducer and drive mechanisms are the two primary components of the drive module, as shown in Figure 9. The driving mechanism supplies energy when the robot moves through a pipeline. The reducer mechanism helps the robot to adjust to the pipeline. The drive module is the fundamental piece required to finish exploring the pipes. Thus, it must have the simultaneous qualities of high power, high reducer, and small size. Table 2

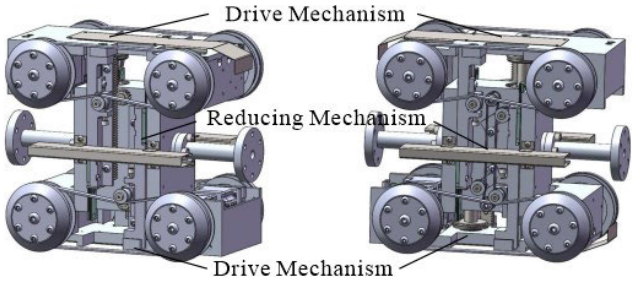

FIGURE 9. The structure of the drive module.

TABLE 2. The parameters of the drive module.

Project	Index
Length	308mm
Width	182mm
Height	180mm
Quality	17.5kg
Applicable pipe diameter	250-450mm

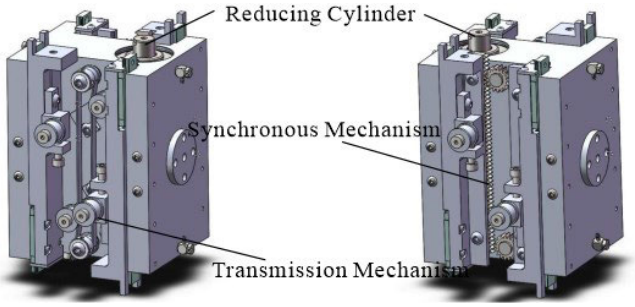

FIGURE 10. The structure of the reducer mechanism.

lists the dimensional parameters of the drive module, which meet the dimensional requirements of the previous section.

The drive module is the fundamental piece required to finish exploring the pipes. Thus, it must have the simultaneous qualities of high power, high reducer, and small size. Table 2 lists the dimensional parameters of the drive module that meet the dimensional requirements of the previous section.

1) STRUCTURAL DESIGN OF REDUCER MECHANISM

As shown in Figure 10, the reducer mechanism consists of three major components: the reducer cylinder, synchronization mechanism, and transmission mechanism. The reducer mechanism is symmetrically distributed at the center. The reducer cylinder stretched along the radial direction of the pipe. The slider moves up and down along the guide rail, whereas the cylinder is stretched, with the guide rail bearing the majority of the lateral force. The rack moved in tandem with the movement of the slider. The two racks mesh with two pinions to ensure that the cylinder telescopes in opposite directions have the same stroke. Consequently, with a good alignment and smooth pressure between the rubber wheel and pipe wall, the distance between the upper and lower driving mechanisms to the center cylinder is the same. It also avoids disengagement due to long travel periods. A drive

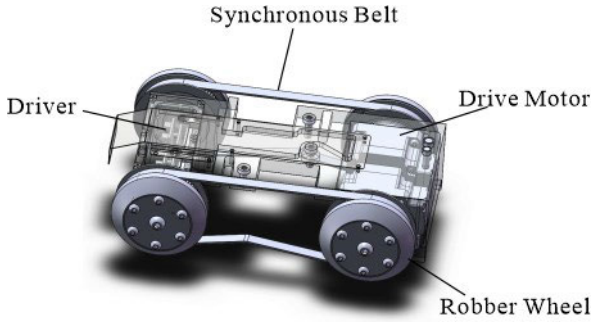

FIGURE 11. The structure of the drive mechanism.

mechanism was mounted on the other side of the two gear shafts. The drive mechanism employs a timing belt drive to ensure smooth and accurate engagement.

2) STRUCTURAL DESIGN OF DRIVE MECHANISM

The structure of the driving mechanism is shown in Figure 11. The driving element of the drive mechanism consists of two drive motors installed on the support plate, each with an independent drive. To minimize the transmission loss and increase the output speed to increase the walking speed of the pipeline robot, the gearbox of the motor was directly connected to the drive wheel. The reducer mechanism squeezes a rubber wheel against the inner wall of the pipe. The drive motor turns to push the rubber wheel to rub against the inner wall of the pipe and produces a driving force. As a result, the driving force is dependent on both the pressure produced by the reduction mechanism's cylinder and the torque of the motor itself. To prevent the driving force from being reduced when passing through the bend because part of the rubber wheel is not in contact with the pipe wall, which affects the robot's passing ability, the rubber wheel without a direct motor drive is connected to the drive motor by a timing belt. Therefore, an additional timing belt is more advantageous for the passing ability of the robot at the bend.

C. ASSEMBLY OF ROBOTS WITH DIFFERENT FUNCTIONS

The pipeline robot assembly was installed in a specific combination for diverse operating situations. The modules were joined by double universal joints to ensure the robot's bending-passing ability. Simultaneously, each module is linked with a quick-change pneumatic and electrical connector in the center to enable efficient installation and disassembly. Based on the various operation methods, the pipeline robots were separated into six operation techniques, as shown in Figure 12.

The six operation techniques were correlated to various operating circumstances inside the pipe. In Figure 12(a), the robot is utilized to clamp large foreign items inside the pipe to ensure its passing ability. Figure 12(b) shows the robot surveys of the pipeline's interior to determine the pipeline internal conditions of the pipeline. In Figure 12(c), By inserting a scanner into the pipeline, the geometric parameters of the pipeline can be obtained by inserting a scanner into the

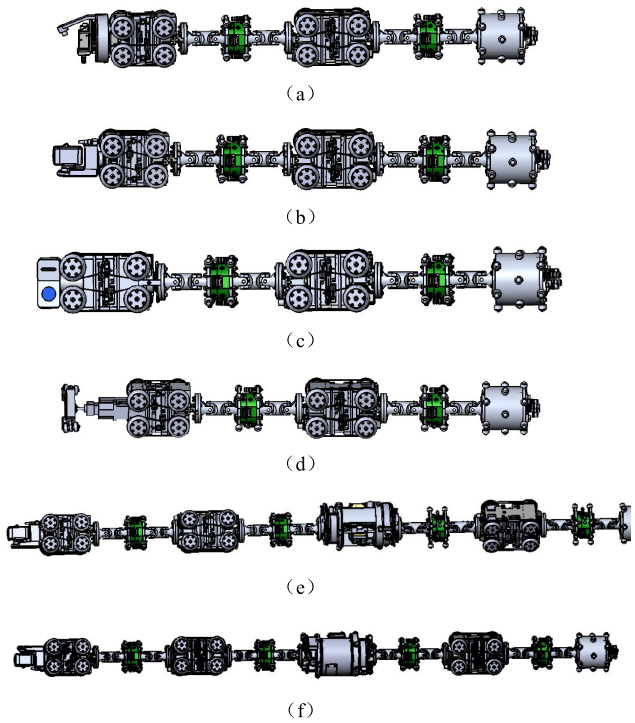

FIGURE 12. Six types of operations.

pipeline. As shown in Figure 12(d), it is mostly utilized to overcome the T-pipe passing ability and assist the pipeline robot in passing through the T-pipe. As shown in Figure 12(e), the robot was capable of performing pipeline weld repairs. As shown in Figure 12(f), the robot could complete the cleaning and collection of small foreign bodies inside the pipe after weld trimming. The connection method was not restricted to these six types of combination methods. Each module and robot can be freely combined to allow for quick disassembly and installation.

IV. ANALYSIS OF THE MOTION OF THE DRIVE MODULE IN THE BEND

When traveling through the bent tube, the robot transitioned from a straight tube to a bent tube to a straight tube. The process of the robot entering the bend from the straight tube is similar to that of the robot entering the straight tube from the bend. This is known as the transition stage. The state in which the robot completely enters the bend is known as the rotation stage. This study examined the motion of the drive module through a curve to make the analysis more straightforward.

A. ANALYSIS OF THE TRANSITION PHASE

Rigid-body plane motion was utilized to assess the robot's motion. Figure 13 shows the location of the robot during the transition stage. With the bending center of the bent tube as the origin, the horizontal direction of the forward movement of the robot was in the positive direction of the X-axis. The vertical direction is the positive direction along the Y-axis. Establishment of global coordinate system $O_0\,(X_0, Y_0, Z_0)$.

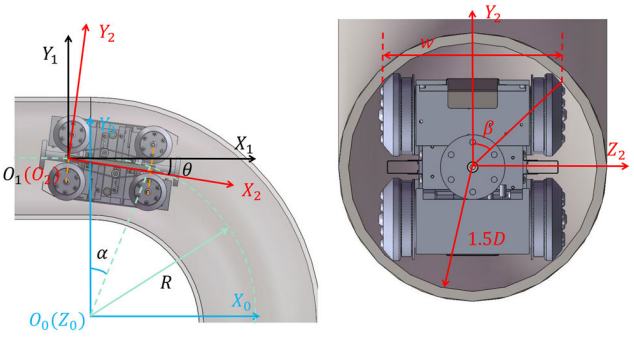

FIGURE 13. Transition stage.

To obtain the transition coordinate system $O_1\,(X_1, Y_1, Z_1)$, the global coordinate system was translated to the center of the four back wheels. Rotate the transition coordinate system clockwise θ around Z_1 to obtain the robot's local coordinate system $O_2\,(X_2, Y_2, Z_2)$. The robot changes from a state in which all wheels are located in a straight tube to the state shown in Figure 13. At this point, the robot's attitude angle is β. The front four wheels turn by an angle of α around the bending center of the curved tube.

The coordinates of the contact point between the front and rear wheels of the robot and tube wall are described in the local coordinate system $O_2\,(X_2, Y_2, Z_2)$:

$$\mathbf{W}_{F2} = \begin{bmatrix} l & l & l & l \\ 0.5D\cos\beta & -0.5D\sin\beta & -0.5D\cos\beta & 0.5D\sin\beta \\ 0.5D\sin\beta & 0.5D\cos\beta & -0.5D\sin\beta & -0.5D\cos\beta \end{bmatrix} \tag{29}$$

$$\mathbf{W}_{R2} = \begin{bmatrix} 0 & 0 & 0 & 0 \\ 0.5D\cos\beta & -0.5D\sin\beta & -0.5D\cos\beta & 0.5D\sin\beta \\ 0.5D\sin\beta & 0.5D\cos\beta & -0.5D\sin\beta & -0.5D\cos\beta \end{bmatrix} \tag{30}$$

l is the distance between the wheel centers at the front and back ends of the robot.

The rotation transformation matrix from the transition coordinate system $O_1\,(X_1, Y_1, Z_1)$ to the local coordinate system $O_2\,(X_2, Y_2, Z_2)$ is.

$$\mathbf{R}_1 = Rot\,(Z_1, -\theta) = \begin{bmatrix} \cos\theta & \sin\theta & 0 \\ -\sin\theta & \cos\theta & 0 \\ 0 & 0 & 1 \end{bmatrix} \tag{31}$$

The translation vector from the global coordinate system $O_0\,(X_0, Y_0, Z_0)$ to the transition coordinate system $O_1\,(X_1, Y_1, Z_1)$ is:

$$\mathbf{T}_0 = \begin{bmatrix} R\sin\alpha - \sqrt{l^2 - R^2\,(1-\cos\alpha)^2} \\ R \\ 0 \end{bmatrix} \tag{32}$$

From the geometric relationship, the following equation can be obtained:

$$l\sin\theta = R\,(1-\cos\alpha) \tag{33}$$

According to [36], the coordinates of the contact point between the front and back wheels of the robot and the

tube wall are described in the global coordinate system $O_0\,(X_0, Y_0, Z_0)$ as:

$$\begin{cases} \mathbf{W}_F = \mathbf{R}_1\mathbf{W}_{F2} + \mathbf{T} \\ \mathbf{W}_R = \mathbf{R}_1\mathbf{W}_{R2} + \mathbf{T} \end{cases} \tag{34}$$

$\mathbf{T}$ is the translation matrix:

$$\mathbf{T} = \begin{bmatrix} \mathbf{T}_0 & \mathbf{T}_0 & \mathbf{T}_0 & \mathbf{T}_0 \end{bmatrix} \tag{35}$$

The velocity matrix of the contact point between the front and back wheels of the robot and the tube wall is described in the global coordinate system $O_0\,(X_0, Y_0, Z_0)$ as follows:

$$\mathbf{V}_F = \frac{d\mathbf{W}_F}{dt} = \begin{bmatrix} v_{fx1} & v_{fx2} & v_{fx3} & v_{fx4} \\ v_{fy1} & v_{fy2} & v_{fy3} & v_{fy4} \\ v_{fz1} & v_{fz2} & v_{fz3} & v_{fz4} \end{bmatrix} \tag{36}$$

$$\mathbf{V}_R = \frac{d\mathbf{W}_R}{dt} = \begin{bmatrix} v_{rx1} & v_{rx2} & v_{rx3} & v_{rx4} \\ v_{ry1} & v_{ry2} & v_{ry3} & v_{ry4} \\ v_{rz1} & v_{rz2} & v_{rz3} & v_{rz4} \end{bmatrix} \tag{37}$$

v_{fxi}, v_{fyi}, and v_{fzi} $(i = 1, 2, 3, 4)$ are components of the velocity of the i wheel at the front end of the robot in the X, Y, Z direction of the global coordinate system $O_0\,(X_0, Y_0, Z_0)$. v_{rxi}, v_{ryi}, and v_{rzi} $(i = 1, 2, 3, 4)$ are the components of the velocity of the i wheel at back end of the robot in the X, Y, Z direction of the global coordinate system $O_0\,(X_0, Y_0, Z_0)$.

The velocity of the magnitude of the robot's front and back wheels at the point of contact with the pipe is.

$$\begin{cases} v_{fi} = \sqrt{v_{fxi}^2 + v_{fyi}^2 + v_{fzi}^2} \\ v_{ri} = \sqrt{v_{rxi}^2 + v_{ryi}^2 + v_{rzi}^2} \end{cases} \tag{38}$$

The robot should control the speed ratio of wheels equal to the curvature of bend ratio when entering the bending process. However, in this design, the front and back wheels are connected with synchronous belts, which results in the same speed of the front and back wheels. It inevitably leads to the generation of internal consumption. To reduce internal consumption, the robot should pass the bent tube at a low speed.

B. ANALYSIS OF THE ROTATION PHASE

Figure 14 shows the rotation phase of the robot. This analysis is similar to that of the transition phase. During the rotation phase, the robot revolved around the Z axis of the global coordinate system. The speeds of the front and back wheels were the same because they were connected by the same timing belt. Two wheels connected by the same timing belt were considered as a single unit. To reduce the internal consumption and promote smoothness, the speed ratio of each wheel should be equal to the curvature ratio of the point between each wheel and the inner wall of the pipe.

$$n_1 : n_2 : n_3 : n_4 = R_1 : R_2 : R_3 : R_4\,(i = 1, 2, 3, 4) \tag{39}$$

n_i and R_i are the i-th wheel's speed and the radius of curvature of the i-th point between the wheel and the pipe's inner wall, respectively.

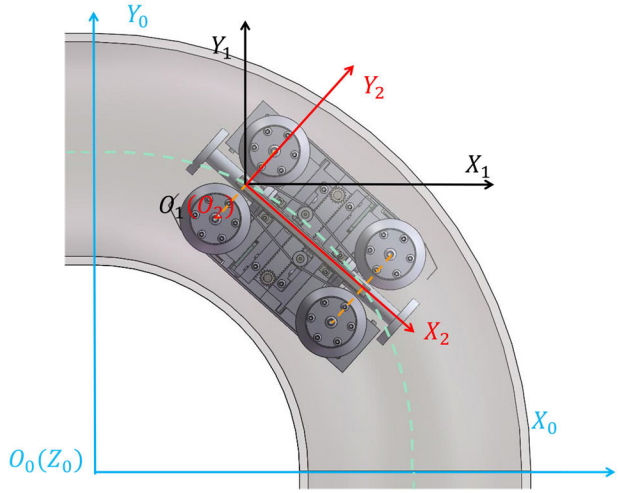

FIGURE 14. Rotating stage.

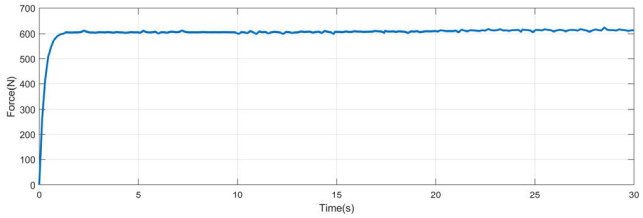

FIGURE 15. Traction of the drive module.

C. ANALYSIS OF THE TRANSITIONAL MOTION

In the process of moving forward, the drive module may twist around the pipe axis, which is harmful to the function of the robot and should be avoided as much as possible. When rotating body motion occurs, the combined moment of the drive module in the forward direction should be 0.

$$\begin{aligned} \sum M = &\sum_{i=1}^{8} F_{ni} \cdot \mathbf{n}_{ni} \cdot \mathbf{e}_Z \cdot y_i + \sum_{i=1}^{8} F_{fi} \cdot \mathbf{n}_{fi} \cdot \mathbf{e}_Z \cdot y_i \\ &+ \sum_{i=1}^{2} F_{qiZ} \cdot y_{qi} - \sum_{i=1}^{8} F_{ni} \cdot \mathbf{n}_{ni} \cdot \mathbf{e}_Y \cdot z_i \\ &- \sum_{i=1}^{8} F_{fi} \cdot \mathbf{n}_{fi} \cdot \mathbf{e}_Y \cdot z_i - \sum_{i=1}^{2} F_{qiY} \cdot z_{qi} \neq 0 \end{aligned} \tag{40}$$

F_{ni} is the normal force acting on a wheel. F_{fi} represents the lateral friction of the wheel. $\mathbf{n}_{ni}$ is the unit vector of the normal force F_{ni} at the contact point of the wheel in the local coordinate system $O_2\,(X_2, Y_2, Z_2)$. $\mathbf{n}_{fi}$ is the unit vector of the lateral friction F_{fi} of the wheel in the local coordinate system $O_2\,(X_2, Y_2, Z_2)$. $\mathbf{e}_Y$ and $\mathbf{e}_Z$ are the unit vectors of coordinate system $O_2\,(X_2, Y_2, Z_2)$ in the positive direction of the two coordinate axes. y_{qi} and z_{qi} are the coordinate values of y and z, respectively, of the universal joint connection in the $O_2\,(X_2, Y_2, Z_2)$ coordinate system.

The normal force F_{ni} of the inner wall on the wheel and the frictional force F_{fi} can be observed to influence the rotation of the robot, and they are unrelated to the interaction

forces F_{qi}. A thorough mechanical examination of the drive module revealed that the combined moment around the forward direction is proportional to the attitude angle β of the robot entering the pipeline. It is stable at a minimum value if it enters the pipe at a stable attitude angle. A small amount of rotational motion occurred. If the robot does not enter the pipe with a stable attitude angle, it rotates, and its attitude angle finally converges to a stable attitude angle.

V. VERIFICATION OF VIRTUAL SIMULATION MODEL

The primary goal of this study was to realize the function of a pipeline robot to complete its operation in a pipeline. The robot can adapt to variations in the pipe diameter range of 250-450mm, pass through a bend with 1.5D radius of curvature, and travel forward in a vertical pipeline. The virtual prototype was simulated using ADAMS software to check the traction force magnitude of the drive module as the core of the overall robot, as well as its motion characteristics and general passing ability.

A. TRACTION ANALYSIS

The drive module must produce a sufficient traction force to transport the tool while ensuring that the entire pipeline robot moves normally. When the air pump's input pressure is 0.5 MPa, the output force of the reducer cylinder of the drive module is approximately 628 N. As shown in Figure 15, a spring was added at the end of the drive module. The stiffness coefficient of the spring was increased to 105 N/m to ensure that it was within the elastic deformation range. The deformation of the spring under the traction of the drive module was very small. When the drive module stopped moving forward, the maximal traction force generated and the reaction force of the spring were equal in size. It stabilizes at approximately 600 N, which satisfies the design requirement of being able to drive the work module.

B. PASSING ABILITY OF THE DRIVE MODULE IN THE BEND

The pass-by simulation of the drive module was validated using a curve with a pipe diameter of 250 mm and a radius of curvature of 1.5 times the pipe diameter. During the passage of the drive module through the bend, the speed of each wheel was set at 10 rpm, resulting in low speed. Figure 16 shows a comparison simulation of the drive module through the bend at different attitude angles. The drive modules are shown in Figures (a), (b), and (c), flowing through the vertical curve at 0°, 30°, and 60°. The robot rotates almost 0° when traversing the bend with an attitude of 0° angle because the wheel end surface is parallel to the plane where the pipe axis is located and the wheel section fits into the bent part of the pipe. When crossing the bend with other postures, it is clear that a turning motion occurred. Consequently, to ensure the stability of the robot's operation, the robot's attitude when crossing the bent pipe should be as close to 0° as possible.

According to the analysis in Section III of this paper, when the pipeline robot runs in the bend, the speed of each driving wheel must be configured to minimize the loss caused by the different turning radii during the turn. The speed of the wheel part is related to the turning radius. The speed of each drive wheel was the same at the start of the robot's trip in the straight tube, as shown in Figure 17. It fluctuated when it entered the transition phase. When the robot enters the rotation phase, the speed remains constant, because the turning radius of the driving wheels does not change at a specific bend in the tube. The driving wheels were operated at two different speeds.

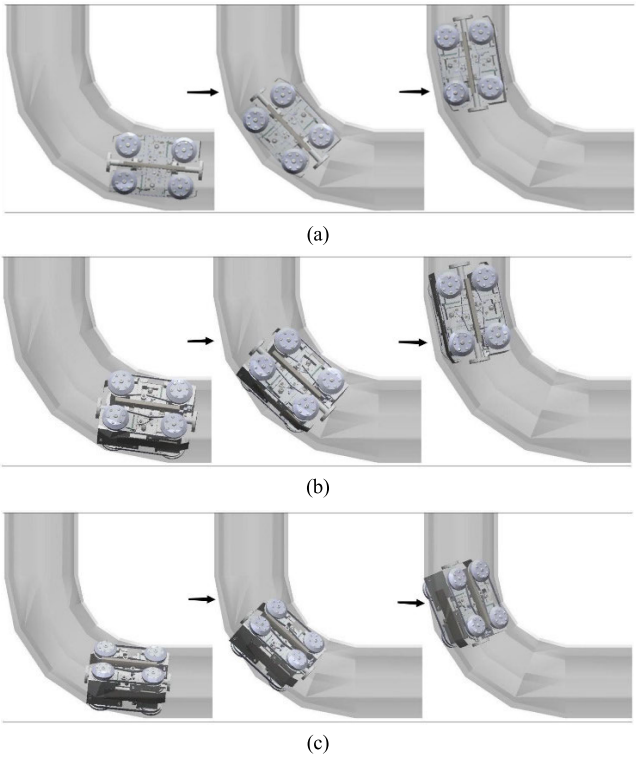

FIGURE 16. The state of the drive module over the bend for different attitude angles.

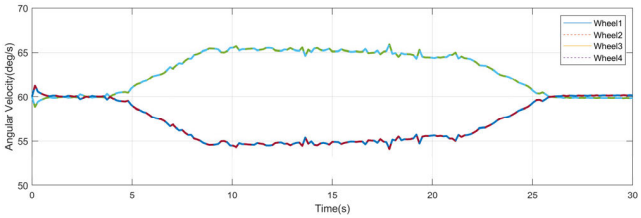

FIGURE 17. Ideal speed diagram for robot over bend.

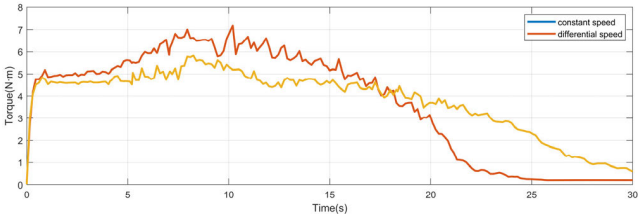

FIGURE 18. Comparison of motor torque at 0° attitude angle.

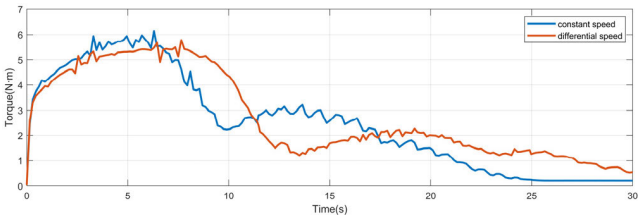

FIGURE 19. Comparison of motor torque at 30° attitude angle.

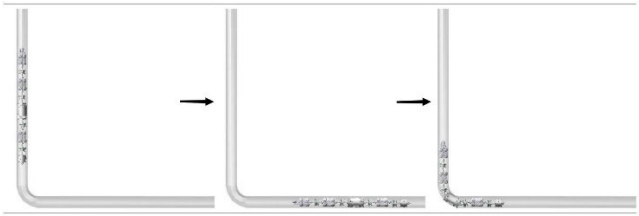

FIGURE 20. Modular robot over vertical bend.

TABLE 3. Active wheel speed configuration.

Project	Index
Direct management phase	60
Transition phase	10
Outer wheel in the rotation phase	50
Inner wheel in the rotation phase	30

If the drive module does not match the speed of each active wheel according to the speed characteristics but maintains an equal speed, it can pass over the bend. The simulation illustrates that the motor torque differs between the two approaches to bending. Figures 18 and 19 compare the motor torque when travelling through the bend with comparable speed and velocity characteristics at attitude angles of 0° and 30°, respectively. When passing at the same speed, independent of the attitude angle through the bend, the motor torque peak and fluctuation degree increase greatly. When negotiating the bend with speed characteristics, the motor torque remains smooth and has a lower peak in the rotation phase, reducing internal consumption and increasing motion smoothness.

C. PASSING ABILITY OF THE SERPENTINE ROBOT IN THE BEND

The modular pipe-working robot has a drive module as the main body, and each module is connected by a universal joint and quick change. Passing ability was simulated and verified. The gimbal constraint was added to the modules in the ADAMS software. The simulation results were verified in a pipe bend with a diameter of 250 mm and a radius of curvature of 1.5 times the pipe diameter as shown in Figure 20. The pipe-working robot smoothly passed through the bend.

VI. EXPERIMENTAL STUDY ON THE SERPENTINE ROBOTS IN PIPELINES

To test the passing ability of the pipeline robot for straight and bent pipes with inner diameters of 250 mm-450 mm, an experimental platform comprising pipes with inner diameters of 250 mm and 450 mm, was constructed, as illustrated in Figure 21. The combined pipes were composed of straight pipes, T-shaped pipes, and bent pipes with flanged edges that could be bolted together. The bent pipes are arranged vertically. The T-pipes were horizontally oriented.

FIGURE 21. Experimental platform.

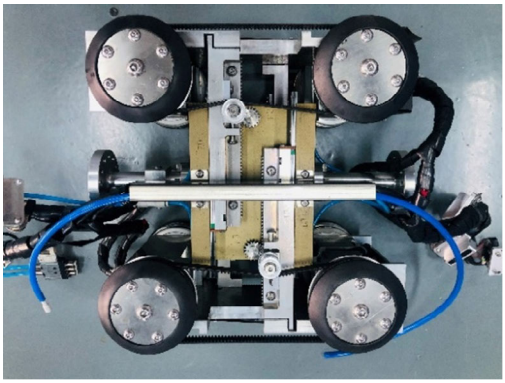

FIGURE 22. Drive module prototype.

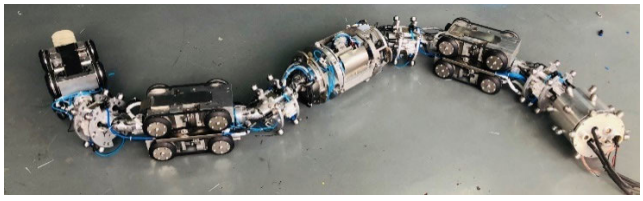

FIGURE 23. Robot prototype.

FIGURE 24. Robot passing through a 250mm combination pipe.

FIGURE 25. Robot passing through a 450mm combination pipe.

TABLE 4. Robot performance.

Project	Index
Passing time in the straight tube /s	5.2
Passage time in the bend/s	4.3
The average velocity of the straight pipe / (m/s)	0.29
The average speed of the bend/(m/s)	0.14
Traction force/N	594

Figure 22 shows the prototype of the manufactured drive module. The main body of the pipeline robot, which is freely constructed in a serpentine form, is shown in Figure 23. The camera operation, drive, grinding operation, drive, and sensing and monitoring modules comprise this modular robot. All modules are connected to the drive module either directly or via universal joints and undergo quick changes.

A modular pipeline robot passing ability test was conducted to evaluate the passing ability of the drive module in the pipeline. Because the pipeline was opaque, observations were made and recorded at the entrance of the pipeline and the opening of the T-shaped pipeline. The process of passing through the 250 mm and 450 mm pipelines is depicted in Figures 24 and 25, respectively.

Table 3 lists the active wheel-speed arrangement of the drive module during the experiments. Each active wheel in the straight tube was set at the same speed. The active wheels pass at low speed during the transition phase. During the rotation phase, each active wheel speed satisfies the corresponding speed-matching relationship, where the wheel speed ratio equals the ratio of the radius of curvature of the contact points. The experiments showed that the modular pipework robot could smoothly pass through a pipe with a combination of straight and bent pipes. The drive module is also bound to pass. Table 4 displays the performanceof the robot in the experimental pipe. Owing to the limitation of the internal space of the bent pipe, the robot could travel faster in a straight pipe and slower in a bent pipe. In the trial, the robot's traction force was measured as 594N, ensuring the ability to pull the operating module and tail cable forward.

The pipeline robot proposed in this paper has a significantly larger reducer range than the other designs in the first section of this paper. It could achieve a reducer range of 250-450 mm (reducer factor of 0.8). Compared with many robots with insufficient traction force, the proposed pipeline robot has a traction force of 594 N, which is fully capable of driving other modules to climb vertical pipes and perform various related operations.

VII. CONCLUSION

In this paper, the following conclusions were drawn:

(1) A snake robot that has multiple functions and can adapt to pipe diameters of 250-450 mm, is designed in this study. This enhances the adaptability of the robot.

(2) A geometric technique was used to construct a mathematical model of a rectangular pipe robot. The vector method was used to assess the limitations of the rectangular pipe robot by bending. The size limit of the over-bend pipe was derived.

(3) A working prototype of the robot was built and tested. The test validated the passing performance of the pipe robot and established the accuracy of the bend-passing hypothesis.

In addition to the wide range of pipe diameter adaptability and large traction force, the pipeline robot proposed in this study is capable of a quick changeover function between each module. This also means that more multifunctional modules can be designed to connect with the current modules, according to the requirements of subsequent research. Thus, the pipeline robot proposed in this study has great potential for use in other fields. For example, one of the difficulties in the field of arc fault detection is that electrical distribution lines are usually routed in pipes, which are very secretive and it is difficult to determine their fault points. A module for arc-fault detection can be developed. It is connected to the robot in this study to complete the detection.

REFERENCES

[1] W. M. F. Al-Masri, M. F. Abdel-Hafez, and M. A. Jaradat, "Inertial navigation system of pipeline inspection gauge," *IEEE Trans. Control Syst. Technol.*, vol. 28, no. 2, pp. 609–616, Mar. 2020.

[2] S. Yang, K. Jeon, D. Kang, and C. Han, "Accident analysis of the Gumi hydrogen fluoride gas leak using CFD and comparison with post-accidental environmental impacts," *J. Loss Prevention Process Industries*, vol. 48, pp. 207–215, Jul. 2017.

[3] Y. Gong and Y. Li, "STAMP-based causal analysis of China-Donghuang oil transportation pipeline leakage and explosion accident," *J. Loss Prevention Process Industries*, vol. 56, pp. 402–413, Nov. 2018.

[4] X. Yang, P. Bai, X. Shen, Z. Li, and Q. Yin, "Design and modeling of a walking mechanism for the self-adapting pipeline robot," *IOP Conf. Ser., Earth Environ. Sci.*, vol. 186, no. 5, 2018, Art. no. 012035.

[5] Z. Wu, Y. Wu, S. He, and X. Xiao, "Hierarchical fuzzy control based on spatial posture for a support-tracked type in-pipe robot," *Trans. Can. Soc. Mech. Eng.*, vol. 44, no. 1, pp. 133–147, Mar. 2020.

[6] T. Li, S. Ma, B. Li, M. Wang, Z. Li, and Y. Wang, "Development of an in-pipe robot with differential screw angles for curved pipes and vertical straight pipes," *J. Mech. Robot.*, vol. 9, no. 5, Oct. 2017, Art. no. 051014.

[7] D. Rollinson and H. Choset, "Pipe network locomotion with a snake robot," *J. Field Robot.*, vol. 33, no. 3, pp. 322–336, 2016.

[8] D. Fang, J. Shang, Z. Luo, P. Lv, and G. Wu, "Development of a novel self-locking mechanism for continuous propulsion inchworm in-pipe robot," *Adv. Mech. Eng.*, vol. 10, no. 1, Jan. 2018, Art. no. 168781401774940.

[9] J. Xudong, S. Qihai, and T. Xiaoyan, "Dynamic characteristics analysis for an in-pipe robot driven by pressure difference based on CEL approach," *J. Vib. Shock*, vol. 38, no. 23, pp. 259–264&270, 2019.

[10] A. Kakogawa, T. Nishimura, and S. Ma, "Designing arm length of a screw drive in-pipe robot for climbing vertically positioned bent pipes," *Robotica*, vol. 34, no. 2, pp. 306–327, Feb. 2016.

[11] L. Brown, J. Carrasco, and S. Watson, "Autonomous elbow controller for differential drive in-pipe robots," *Robotics*, vol. 10, no. 1, p. 28, Feb. 2021.

[12] X. Liu, S. Zhang, Q. Ding, X. Zhu, S. Chen, and Y. Wang, "Design of wireless and self-adaptive oil-gas pipeline traction robot," in *Proc. 2nd Int. Conf. Artif. Intell. Inf. Syst.*, May 2021, pp. 1–6.

[13] P. Li, M. Tang, C. Lyu, M. Fang, X. Duan, and Y. Liu, "Design and analysis of a novel active screw-drive pipe robot," *Adv. Mech. Eng.*, vol. 10, no. 10, Oct. 2018, Art. no. 168781401880138.

[14] G. Mills, A. Jackson, and R. Richardson, "Advances in the inspection of unpiggable pipelines," *Robotics*, vol. 6, no. 4, p. 36, Nov. 2017.

[15] Z. Song, H. Ren, J. Zhang, and S. S. Ge, "Kinematic analysis and motion control of wheeled mobile robots in cylindrical workspaces," *IEEE Trans. Autom. Sci. Eng.*, vol. 13, no. 2, pp. 1207–1214, Apr. 2016.

[16] M. A. A. Wahed and M. R. Arshad, "Wall-press type pipe inspection robot," in *Proc. IEEE 2nd Int. Conf. Autom. Control Intell. Syst. (ICACIS)*, Kota Kinabalu, Malaysia, Oct. 2017, pp. 185–190.

[17] Y.-G. Kim, D.-H. Shin, J.-I. Moon, and J. An, "Design and implementation of an optimal in-pipe navigation mechanism for a steel pipe cleaning robot," in *Proc. 8th Int. Conf. Ubiquitous Robots Ambient Intell. (URAI)*, Nov. 2011, pp. 772–773.

[18] G. Feng, W. Li, H. Zhang, Z. Li, and Z. He, "Development of a wheeled and wall-pressing type in-pipe robot for water pipelines cleaning and its traveling capability," *Mechanics*, vol. 26, no. 2, pp. 134–145, Apr. 2020.

[19] H. Yan, L. Wang, P. Li, Z. Wang, X. Yang, and X. Hou, "Research on passing ability and climbing performance of pipeline plugging robots in curved pipelines," *IEEE Access*, vol. 8, pp. 173666–173680, 2020.

[20] A. Kakogawa and S. Ma, "An in-pipe inspection module with an omnidirectional bent-pipe self-adaptation mechanism using a joint torque control," in *Proc. IEEE/RSJ Int. Conf. Intell. Robots Syst. (IROS)*, Macau, China, Nov. 2019, pp. 4347–4352.

[21] H. M. Kim, Y. S. Choi, Y. G. Lee, and H. R. Choi, "Novel mechanism for in-pipe robot based on a multiaxial differential gear mechanism," *IEEE/ASME Trans. Mechatronics*, vol. 22, no. 1, pp. 227–235, Feb. 2017.

[22] A. Hadi, A. Hassani, K. Alipour, R. A. Moghadam, and P. P. Niaz, "Developing an adaptable pipe inspection robot using shape memory alloy actuators," *J. Intell. Mater. Syst. Struct.*, vol. 31, no. 4, pp. 632–647, Mar. 2020.

[23] Z.-L. Xu, S. Lu, J. Yang, Y.-H. Feng, and C.-T. Shen, "A wheel-type in-pipe robot for grinding weld beads," *Adv. Manuf.*, vol. 5, no. 2, pp. 182–190, Jun. 2017.

[24] Q. Tu, Q. Liu, T. Ren, and Y. Li, "Obstacle crossing and traction performance of active and passive screw pipeline robots," *J. Mech. Sci. Technol.*, vol. 33, no. 5, pp. 2417–2427, May 2019.

[25] Y. Tamura, I. Kanai, K. Yamada, and H.-O. Lim, "Development of pipe inspection robot using ring-type laser," in *Proc. 16th Int. Conf. Control, Autom. Syst. (ICCAS)*, Gyeongju, (South) Korea, Oct. 2016, pp. 211–214.

[26] H. Jang, T. Y. Kim, Y. C. Lee, Y. S. Kim, J. Kim, H. Y. Lee, and H. R. Choi, "A review: Technological trends and development direction of pipeline robot systems," *J. Intell. Robotic Syst.*, vol. 105, no. 3, p. 59, Jul. 2022.

[27] M. N. Mohammed, V. S. Nadarajah, N. F. M. Lazim, N. S. Zamani, O. I. Al-Sanjary, M. A. M. Ali, and S. Al-Youif, "Design and development of pipeline inspection robot for crack and corrosion detection," in *Proc. IEEE Conf. Syst., Process Control (ICSPC)*, Melaka, Malaysia, Dec. 2018, pp. 29–32.

[28] D. Waleed, S. H. Mustafa, S. Mukhopadhyay, M. F. Abdel-Hafez, M. A. K. Jaradat, K. R. Dias, F. Arif, and J. I. Ahmed, "An in-pipe leak detection robot with a neural-network-based leak verification system," *IEEE Sensors J.*, vol. 19, no. 3, pp. 1153–1165, Feb. 2019.

[29] H. Li, R. Li, J. Zhang, and P. Zhang, "Development of a pipeline inspection robot for the standard oil pipeline of China national petroleum corporation," *Appl. Sci.*, vol. 10, no. 8, p. 2853, Apr. 2020.

[30] R. Summan, W. Jackson, G. Dobie, C. MacLeod, C. Mineo, G. West, D. Offin, G. Bolton, S. Marshall, and A. Lille, "A novel visual pipework inspection system," in *Proc. AIP Conf.*, 2018, pp. 1–9.

[31] L. Fanghua and S. Wei, "Analysis and simulation of the passability of adaptive pipe grinding robot," *Mach. Tool Hydraul.*, vol. 49, no. 21, pp. 15–21, 2021.

[32] Z. Cai, C. Lin, D. Huo, and C. Zhu, "Design and analysis of cleaning mechanism for an intermittent screw-driven pipeline robot," *J. Mech. Sci. Technol.*, vol. 31, no. 2, pp. 911–921, Feb. 2017.

[33] W. Hongchong and L. Xiu, "Analysis on traveling capability of pipeline robot in syphon," *Mech. Manuf. Autom.*, vol. 36, no. 4, pp. 57–59, 2007.

[34] H. M. Kim, Y. S. Choi, H. M. Mun, S. U. Yang, C. M. Park, and H. R. Choi, "2–2D differential gear mechanism for robot moving inside pipelines," in *Proc. IEEE/RSJ Int. Conf. Intell. Robots Syst. (IROS)*, Hamburg, Germany, Sep. 2015, pp. 1152–1157.

[35] A. Brunete, A. Ranganath, S. Segovia, J. P. de Frutos, M. Hernando, and E. Gambao, "Current trends in reconfigurable modular robots design," *Int. J. Adv. Robotic Syst.*, vol. 14, no. 3, May 2017, Art. no. 172988141771045.

[36] H. Tourajizadeh and M. Rezaei, "Design and control of a steerable screw in-pipe inspection robot," in *Proc. 4th Int. Conf. Robot. Mechatronics (ICROM)*, Tehran, Iran, Oct. 2016, pp. 98–104.

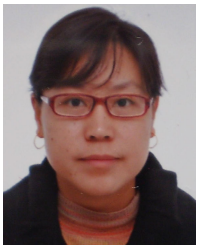

QING LI was born in Hebei, China. She received the bachelor's degree and the Ph.D. degree in mechanical engineering from Tianjin University, China, in 1993 and 2005, respectively. She is currently a Professor and a Master's Supervisor with the School of Mechanical Engineering, Tianjin University. Her research interests include robot design, gear design, complex surface machining, and CNC systems.

WENYA ZHAO was born in Hebei, China. She received the bachelor's degree in engineering from Shandong University, China, in 2021. She is currently pursuing the master's degree in mechanical engineering with Tianjin University, China. Her research interests include pipeline robot and mechatronics.